

Electrothermal tuning of Al–SiC nanomechanical resonators

Seong Chan Jun¹, X M H Huang¹, M Manolidis¹, C A Zorman², M Mehregany² and J Hone¹

¹ Department of Mechanical Engineering and Nanoscale Science and Engineering Center, Columbia University, 500 W. 120 Street, Room 220 Mudd, New York, NY 10027, USA

² Department of Electrical Engineering and Computer Science, Case Western Reserve University, Cleveland, OH 44106, USA

E-mail: jh2228@columbia.edu

Received 21 November 2005, in final form 9 January 2006

Published 16 February 2006

Online at stacks.iop.org/Nano/17/1506

Abstract

A highly effective electrothermal tuning method is demonstrated for Al–SiC nanomechanical resonators. Doubly clamped beam devices are actuated and read out using a magnetomotive technique under a moderate vacuum at room temperature. Direct current applied to a beam heats the structure and shifts the resonance frequency downward. Frequency shifts of 10% are easily achievable, and the thermal time constant of these structures is in the submicrosecond range. The initial frequency and frequency tunability are studied for beams of varying Al thickness, and the device performance can be accurately modelled using simple mechanical and thermal models. Because of the different mechanical properties of SiC and Al, both the initial frequency and the frequency tunability can be modified by varying the Al layer thickness. This approach has the potential to become an important tool for effective frequency tuning in deployable SiC-based nanoelectromechanical system devices and systems for applications that would benefit from SiC as the structural material.

(Some figures in this article are in colour only in the electronic version)

1. Introduction

Nanoelectromechanical systems (NEMS) offer great promise for applications in mechanical signal processing and ultra-sensitive detection [1–4]. As device dimensions are reduced, the frequency of NEMS devices can reach the MHz to GHz regime. At the same time, the small size of the devices ensures low operating power, high responsivity and parameter tunability. SiC has emerged as a versatile structure material for NEMS devices. Its high Young's modulus-to-density ratio has proven advantageous for improving the performance of ultrahigh and microwave frequency nanomechanical resonators [5], which in turn are demonstrated to be useful for a number of important research directions, including nanomechanical mass detection [6], mechanical parametric amplification and the prototyping of devices for quantum measurement [7]. A number of methods, including magnetomotive transduction, optical interferometry and capacitive detection, have been used to detect device

motion, but readout in general represents a primary challenge in the NEMS field. In the examples cited above, a magnetomotive transduction technique was used to excite the resonators and measure their response. The required high magnetic field was provided by a superconducting magnet in a cryostat under extremely low-temperature conditions. Such an approach provides excellent experimental performance, but presents a significant obstacle to implementing these devices in many applications. Ideally, this scheme could be used at room temperature and as close as possible to atmospheric pressure. In addition, low-cost portable components are essential for applications.

The ability to tune the frequency of a NEMS device will be crucial for potential applications. On long timescales, tuning will be necessary to compensate for variability in manufacturing and thermal drift. Frequency tuning on short timescales will be necessary for applications such as mechanical signal processing that will require signal tracking, frequency hopping, etc. There are many possible methods

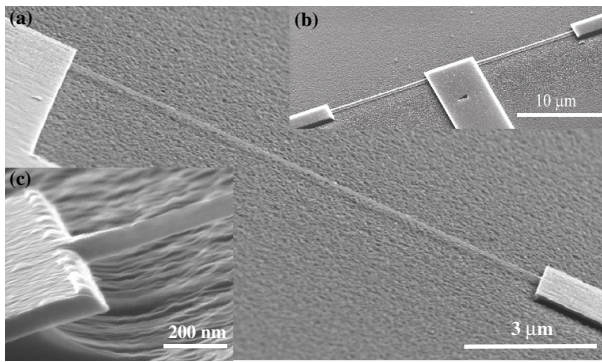


Figure 1. SEM micrographs of a completed device. (a) 12 μm long SiC–Al beam. (b) Two nearly identical beams form a device pair to be tested simultaneously in a balanced electronic circuit. (c) Zoom-in view of one of the resonator beams, clearly showing the suspension of the structure.

for NEMS frequency tuning, including modification of the beam tension by capacitive pull-in or Lorentz force [2]. This paper focuses on electrothermal tuning, which has been widely used for frequency tuning in MEMS devices [8, 9]. As the devices scale down to nanometre sizes, the performance and characteristics of this active tuning method need to be assessed. This paper focuses on the application of electrothermal tuning to composite nanomechanical resonators made from ultrathin (30 nm thick) 3C–SiC and 30–195 nm of aluminium [10, 11].

2. A nanomechanical resonator

Ultrathin single-crystal 3C–SiC films were grown on a silicon wafer by a heteroepitaxial atmospheric pressure chemical vapour (APCVD) process [12]. SiH_4 and C_3H_8 were used as precursors and H_2 as a carrier gas. The epitaxial process is a two-step, high-temperature (1280 $^\circ\text{C}$) procedure, involving the carbonization of the Si surface in a $\text{C}_3\text{H}_8/\text{H}_2$ ambient followed by epitaxial growth using SiH_4 , C_3H_8 and H_2 . The films used in this study were 30 nm thick. The surface roughness of these films was found to be well below 1 nm.

The nanoscale resonators were fabricated using electron-beam (E-beam) lithography combined with reactive ion etching. E-beam lithography, followed by evaporation and lift-off of aluminium, is used to define the device pattern on top of the SiC surface. Reactive ion etching using CF_4/O_2 (9:1), with an RF power of 100 W and gas pressure of 250 mTorr, is used to etch the SiC layer anisotropically. After a total of 2 min of etching, this recipe first clears the silicon carbide film not covered by aluminium, and then etches into the silicon substrate isotropically, thereby releasing the doubly clamped beam device structure. The aluminium layer serves as both an etch mask and a conductive layer for later device testing. The etch rate for aluminium is found to be negligible. A scanning electron micrograph (SEM) image of a 12 μm long beam is shown in figure 1(a), and two nearly identical beams form a device pair to be tested in a balanced electronic circuit in figure 1(b). Figure 1(c) shows a magnified view of one of the resonator beams, and the suspension of the structure can be clearly seen.

3. Device operation

In this resonator, magnetomotive transduction is used for device testing [13–15]. The data presented below were generated in a room-temperature tabletop apparatus that is capable of performing magnetomotive testing on nanomechanical resonators without the need for cryogenic temperatures and superconducting magnets. The operation of this setup has been previously demonstrated [16] for AuPd alloy nanomechanical resonators. The device is wire bonded and loaded into a vacuum chamber that is evacuated by a small dry mechanical pump capable of achieving pressures of ~ 1 Torr, which are sufficient for high- Q operation of the NEMS resonators [17]. Electrical feedthroughs allow connections between the devices and test equipment. An NdFeB permanent magnet is mounted near the device and used for magnetomotive detection of mechanical resonance. The magnet provides a perpendicular field up to 0.9 T at the test chip. The field strength can be varied by mechanically shifting the position of the magnet relative to the sample.

The RF drive and readout is accomplished with a network analyser (HP 3577A). Because the magnetomotive signal [14] varies as B^2 , the signal levels in this system are ~ 100 times smaller than those in a superconducting magnet system for a given beam. However, the magnetomotive signal also varies as L^5/t^3 , where L is the beam length and t is the thickness in the plane of vibration. Therefore, it is possible to modify the beam geometry (by increasing the aspect ratio) to increase the signal to reasonable levels. This necessarily results in a reduction in frequency, but because the frequency is only proportional to t/L^2 it is still possible to attain frequencies in the MHz range.

To further optimize the electrical readout, two resonators are fabricated side-by-side to form an RF resistance bridge [18], as shown in figure 2. The two arms of the bridge are driven out of phase by passing the drive signal through a 180 $^\circ$ power splitter. In this way, the middle arm of the device is at virtual ground until one of the beams is in resonance, so that the background signal is significantly reduced. Frequency tuning of the beams is accomplished electrothermally. A direct current heats the beam, changing the stress in the structure and decreasing the resonant frequency. A bias tee is used to apply the DC tuning voltage in parallel with the RF drive.

4. Device modelling background

4.1. Effects of stress on frequency

The major effect of heating by the DC tuning power is to change the tension in the beam due to thermal expansion. Because the beam is much smaller than the supports, we model the system as a simple doubly clamped beam whose length remains fixed. We first consider a beam composed of a single material, and then generalize the results to the case of a composite beam of SiC and Al.

The resonant natural frequency f_0 of a rectangular doubly clamped beam under zero tension is given by

$$f_0 = 1.03 \frac{w}{L^2} \sqrt{\frac{E}{\rho}} \quad (1)$$

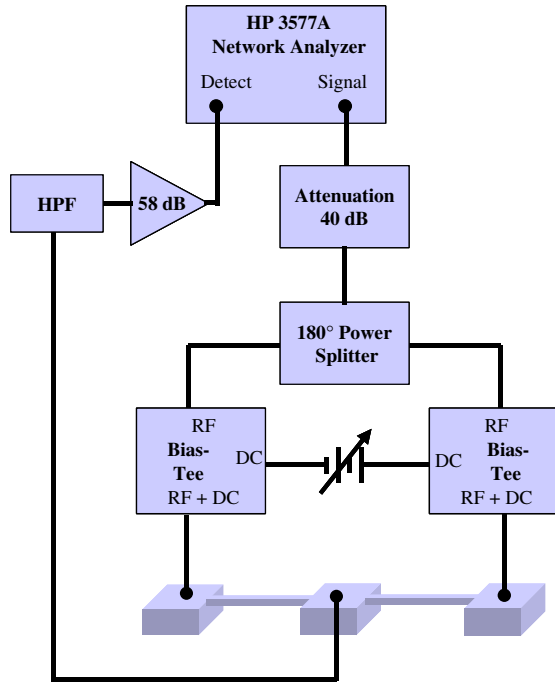


Figure 2. Schematic diagram of the experimental setup.

where w is the beam width in the plane of vibration, L is the length, E is the Young's modulus and ρ is the density. Under stress, the resonant frequency increases according to [19]

$$f(\sigma) = f_0 \sqrt{1 + \frac{\sigma L^2}{3.4 E w^2}} \quad (2)$$

where σ is the tensile stress. In these studies, the stress σ is the sum of the room-temperature built-in stress σ_i resulting from the film deposition process and a thermal stress σ_t from heating of the beam, i.e.

$$\sigma = \sigma_i + \sigma_t = \sigma_i - \alpha E \Delta T \quad (3)$$

where α is the thermal expansion coefficient and ΔT is the average increase in temperature of the beam. The initial (zero heating power) measured frequency is then given by

$$f_i = f_0 \sqrt{1 + \frac{\sigma_i L^2}{3.4 E w^2}} \quad (4)$$

and the tuned frequency is

$$\frac{f}{f_i} = \sqrt{1 + \left(\frac{f_0}{f_i}\right)^2 \frac{\sigma_t L^2}{3.4 E w^2}} \quad (5)$$

For a composite beam, equations (1)–(5) above can be used to predict the behaviour of the beam, with one modification: the values for the Young's modulus, density, stress and thermal expansion coefficient must be replaced by effective values that represent weighted averages of the two materials, each of which has a cross-sectional area A . These effective parameters are as follows:

$$E_e = \frac{E_{SiC} A_{SiC} + E_{Al} A_{Al}}{A_{SiC} + A_{Al}} \quad (6)$$

$$\rho_e = \frac{\rho_{SiC} A_{SiC} + \rho_{Al} A_{Al}}{A_{SiC} + A_{Al}} \quad (7)$$

$$\sigma_e = \frac{\sigma_{Al} E_{Al} A_{Al} + \sigma_{SiC} E_{SiC} A_{SiC}}{E_{Al} A_{Al} + E_{SiC} A_{SiC}} \quad (8)$$

$$\alpha_e = \frac{\alpha_{Al} E_{Al} A_{Al} + \alpha_{SiC} E_{SiC} A_{SiC}}{E_{Al} A_{Al} + E_{SiC} A_{SiC}} \quad (9)$$

4.2. Thermal modelling

The thermal properties of the beam determine both the temperature increase with applied DC power and the thermal response time of the system. Heat transfer is dominated by conduction along the beam, which can be modelled as a bulk system: in spite of the small cross-sectional area, the phonon mean free path is smaller than the beam size at room temperature. Furthermore, because the beam has a high aspect ratio and is much smaller than the supports, we can approximate the system as a one-dimensional heat conduction problem, with a fixed temperature T_0 at the clamping points. At steady state, the temperature of the beam is given by

$$\frac{d^2 T}{dx^2} + \frac{\dot{Q}}{K_e} = 0 \quad (10)$$

where x is the position along the length of the beam, \dot{Q} is the power generated per unit volume and the effective thermal conductivity is given by

$$K_e = \frac{K_{SiC} A_{SiC} + K_{Al} A_{Al}}{A_{SiC} + A_{Al}} \quad (11)$$

The solution to equation (10) gives the temperature change of the beam as a function of position

$$\Delta T(x) = \frac{\dot{Q}}{2 K_e} \left(\frac{L}{2} x^2 - \frac{1}{3} x^3 \right) \quad (12)$$

By averaging equation (12) over the length of the beam, and replacing \dot{Q} with P_e/AL , where A is the cross-sectional area of the beam and $P_e = I^2 R$ is the electrical heat production, we obtain:

$$\Delta T_e = \frac{P_e L}{12 A K_e} \quad (13)$$

Finally, combining equations (5) and (13), we obtain a single expression for the thermal tuning of the beam:

$$\frac{f}{f_i} = \sqrt{1 + \left(\frac{f_0}{f_i}\right)^2 \left(\frac{\alpha_e}{K_e} \times \frac{L^3}{40.8 w^3 h}\right) P_e} \quad (14)$$

To assess the speed of the frequency tuning process, it is necessary to calculate the thermal time constant of the beam. The response of the beam with a time-dependent heat production added can be solved as a Sturm–Liouville problem [20], with

$$T(x, t) - T_0 = \sum_{n=1}^{\infty} a_n(t) \phi_n(x) \quad (15)$$

where $a_n(t)$ are the generalized Fourier coefficients. The time constant of the n th mode is given by:

$$\tau_n = \left(\frac{L}{n\pi}\right)^2 \frac{\rho_e c_e}{K_e} \quad (16)$$

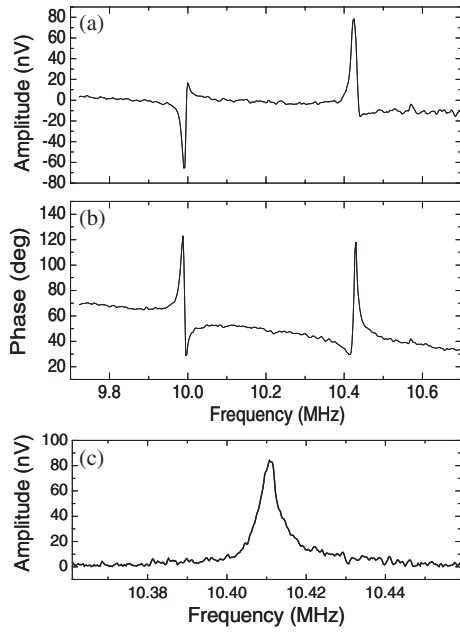


Figure 3. Amplitude (a) and phase (b) traces for a pair of beams driven with $100\ \mu\text{V}$ in a $0.9\ \text{T}$ magnetic field. A deconvoluted single peak (c) shows the signal–noise level achievable in this system.

where c_e is the effective heat capacity of the beam. The lowest ($n = 1$) eigenmode has the longest time constant and will therefore define the minimum thermal response time of the beam.

5. Results

5.1. Resonance at zero tuning power

By plotting the detected electrical signal versus driving frequency, peaks at the mechanical resonance of the beam can be observed. Typical raw amplitude and phase data, with a $100\ \mu\text{V}$ drive, are shown in figures 3(a) and (b). The frequency sweeps show double peaks corresponding to each of the two resonator beams in the device pair. A more detailed study of the upper amplitude peak, with the background subtracted out, is shown in figure 3(c). These data demonstrate that high-frequency NEMS actuation and readout are quite easily accessible at room temperature, moderate vacuum (about 1 Torr) and magnetic fields small enough (under $0.9\ \text{T}$) to be achieved using a permanent magnet. In subsequent sections, the peak of a single beam is tracked to characterize the frequency tuning.

Figure 4 shows the predicted zero-tension resonant frequency f_0 (open symbols) and measured frequency at zero tuning power f_i (solid symbols) of four beams, with Al layer thicknesses of 30, 65, 115 and 195 nm. Young's moduli of 410 and 68 GPa are assumed for SiC and Al, respectively [21–23]. From the calculated and measured frequencies, the initial tensile stress σ_i in the beam can be calculated using equation (4). Figure 5 shows the calculated tensile stress as a function of aluminium thickness for the four beams. The net stress decreases as Al thickness increases, indicating that the Al layer is under compressive stress. Values of σ_{Al} and σ_{SiC} can be obtained by fitting equation (8) to the

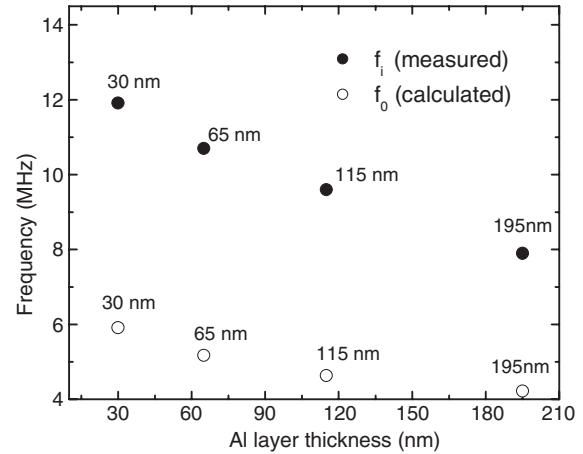


Figure 4. Calculated zero-tension frequency f_0 and measured initial frequency f_i of beams with 30, 65, 115 and 195 nm Al layer thicknesses.

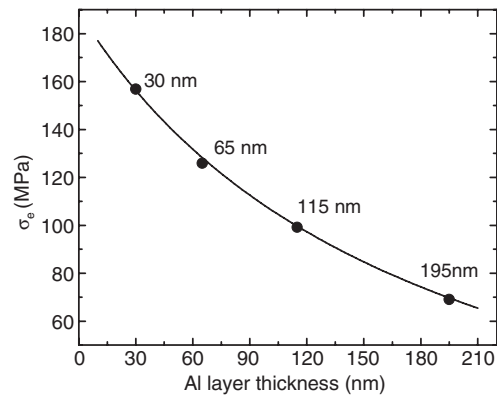


Figure 5. Measured effective stress σ_e of beams with 30, 65, 115 and 195 nm Al layer thicknesses (solid symbols). The solid line represents a fit to the data using equation (5), with values of $\sigma_{\text{Al}} = -49\ \text{MPa}$ and $\sigma_{\text{SiC}} = 189\ \text{MPa}$.

data in figure 5. The best fit, plotted as the solid line in figure 5, is obtained for $\sigma_{\text{Al}} = -49\ \text{MPa}$ and $\sigma_{\text{SiC}} = 189\ \text{MPa}$. Because of the greater stiffness of the SiC beam, its tensile stress provides the dominant contribution. However, it can be seen that changing the Al thickness can be an effective way of modifying the beam stress and therefore the resonant properties.

5.2. Frequency tuning

Figure 6 shows the response of three beams, with Al layers of 65, 115 and 195 nm, to a DC heating power applied on top of a fixed RF drive voltage of $100\ \mu\text{V}$. For all three beams, the frequency decreases nearly linearly with applied DC power, and shifts of $\sim 10\%$ are observed at the highest power levels. The device behaviour was observed to be highly repeatable at the power levels shown, whereas at higher power levels the devices first show hysteretic behaviour and eventually break.

For all of the beams studied, the observed behaviour is independent of RF drive voltage and magnetic field strength; the lack of a magnetic field effect rules out a significant contribution from tension induced by a perpendicular Lorentz

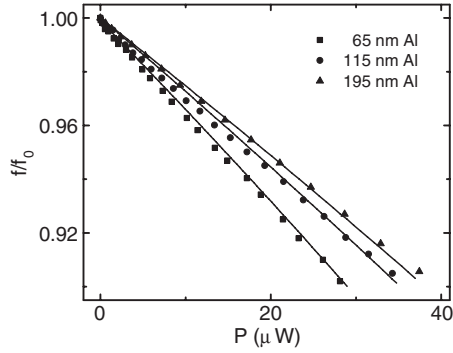


Figure 6. Frequency tuning for beams with 65, 115 and 195 nm aluminium layers. The symbols represent the measured frequency as a function of DC heating power, at 100 μV drive voltage and 0.9 T magnetic field strength. The lines represent theoretical fits to these data using equation (14), with fitting parameters $K_{\text{SiC}} = 360 \text{ W m}^{-1} \text{ K}^{-1}$ and $K_{\text{Al}} = 250 \text{ W m}^{-1} \text{ K}^{-1}$ and the materials parameters summarized in table 1.

Table 1. The material properties of SiC and Al used to model the resonance and frequency tuning response of the beams. The thermal conductivity values are derived by fitting the frequency tuning data to equation (14). All other parameters are standard values for these materials [21–25].

	SiC	Al
Young's modulus (GPa)	410	68
Density (kg m^{-3})	3200	2700
Thermal expansion coefficient (K^{-1})	4×10^{-5}	2.4×10^{-4}
Specific heat ($\text{J kg}^{-1} \text{ }^\circ\text{C}^{-1}$)	690	902
Thermal conductivity ($\text{W m}^{-1} \text{ K}^{-1}$)	360	205

force on the beam. The observed behaviour is highly consistent with a thermally induced reduction in the beam tension, and therefore the system is analysed below in the framework of thermomechanical effects. The RF power that drives the devices into motion is of the order of 10 pW, and thus results in negligible heating of the beams.

The solid lines in figure 6 show theoretical fits to the data using equation (14). For modelling purposes, published values of all materials parameters except thermal conductivity are used, as summarized in table 1. Because thermal conductivity can be highly sample-dependent, the thermal conductivities of SiC and Al are allowed to vary as free parameters. We find that the data for all three beams can be well fitted using $K_{\text{SiC}} = 360 \text{ W m}^{-1} \text{ K}^{-1}$ and $K_{\text{Al}} = 205 \text{ W m}^{-1} \text{ K}^{-1}$. These derived thermal conductivities are well within the range of published data for room-temperature thermal conductivity of these materials [24, 25]. It is good confirmation of the above modelling that good fits to all three curves can be obtained with only two free parameters. In addition, very reasonable thermal conductivities are derived. Independent measurement of the residual film stress and thermal conductivity (under way now) will help strengthen this conclusion.

It is possible to calculate the thermal time constant of the beam using equation (16), the known heat capacity of the two materials in table 1 and the thermal conductivities derived above. The resulting thermal time constant for these beams is $\sim 0.15 \mu\text{s}$, indicating that the bandwidth of the frequency tuning should be as large as $\sim 6 \text{ MHz}$. This high bandwidth

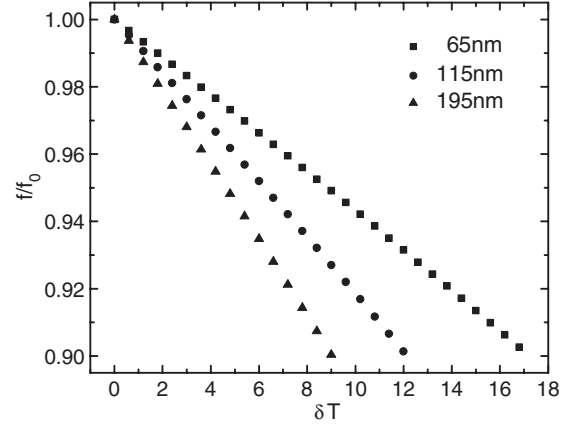


Figure 7. Measured frequency of beams with Al thickness of 65, 115 and 195 nm, as a function of the calculated average temperature rise.

opens up the possibility of performing high-speed frequency modulation, thermomechanical mixing and other novel signal processing techniques. In fact, for beams with slightly different geometry it should be possible to make the thermal time constant shorter than the mechanical oscillation period. The similarity of thermal and mechanical timescales constitutes a unique property of nanoscale devices that has yet to be fully explored or exploited.

Knowing the thermal conductivity of the two materials permits the average temperature rise of the beam as a function of power to be calculated according to equation (13). This permits us to rescale the data to obtain the frequency shift as a function of average temperature increase, as plotted in figure 7. Interestingly, the slope $\partial f/\partial \Delta T$ increases for greater Al thickness. This result can be understood by examining equation (5): the derivative $\partial f/\partial \Delta T$ is larger for beams with a smaller value of the initial (built-in) stress. Because of the compressive stress in the Al beams, the built-in stress is smaller and the frequency response as a function of temperature is greater. Thus, modifying the thickness of the Al layer allows us to change not only the resonant frequency of the beam but also the frequency tunability.

5.3. Quality factor

Figure 8 shows the resonant peak of a beam, normalized to the same frequency, at three different tuning voltages. By fitting the peak to a Lorentzian line shape, the quality factor can be extracted. The initial quality factor of the resonator is about 2000. Upon heating, the quality factor drops by up to $\sim 8\%$, as shown in the inset to figure 8. This decrease is not enough to modify the resonant frequency, but may affect performance for some applications such as signal processing. Examination of this effect is beyond the scope of this paper, but should present an interesting topic for future study.

6. Conclusion

NEMS beams consisting of SiC and Al were fabricated and read out using magnetomotive transduction in a tabletop room-temperature apparatus. The frequency of these beams can be tuned up to $\sim 10\%$ by application of a direct current on

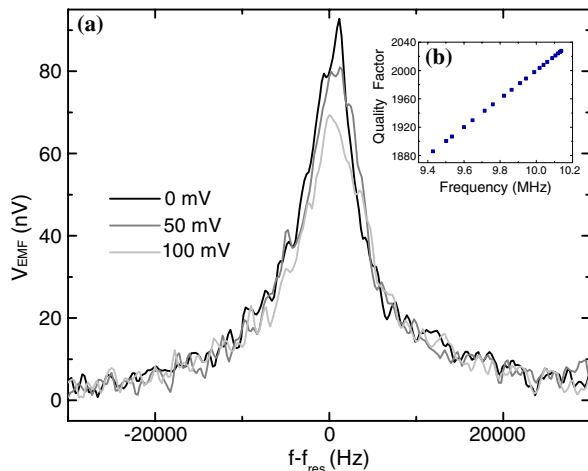


Figure 8. Resonance of the beam at three different tuning voltages. The inset shows the quality factor as a function of resonant frequency.

top of the AC resonant excitation. The tuning effect can be modelled as a modification in the stress in the beam due to thermal expansion. By examining the response of the beams as a function of Al thickness, values for the thermal conductivity of the SiC and Al layers can be extracted, and both values are in good agreement with published data. When the frequency is plotted as a function of temperature increase, it can be seen that the thicker beams show a greater response, as would be expected for beams with lower initial tensile stress. Modification of the beam stress, accomplished in this study by varying the Al layer thickness, can therefore modify both the natural beam resonance and the response of the beam to thermal tuning. The thermal response of these beams is very fast, a unique property of NEMS that point to new modes of device operation.

Acknowledgments

This work was partially supported by the Nanoscale Science and Engineering Initiative of the National Science Foundation

under NSF Award Number CHE-0117752 and by the New York State Office of Science, Technology, and Academic Research (NYSTAR).

References

- [1] Roukes M L 2001 *Sci. Am.* **285** 48
- [2] Ekinici K L and Roukes M L 2005 *Rev. Sci. Instrum.* **76** 061101
- [3] Craighead H G 2000 *Science* **290** 1532
- [4] Nguyen C T C, Katehi L P B and Rebeiz G M 1998 *Proc. IEEE* **86** 1756
- [5] Huang X M H, Zorman C A, Mehregany M and Roukes M L 2003 *Nature* **421** 496
- [6] Ekinici K L, Huang X M H and Roukes M L 2004 *Appl. Phys. Lett.* **84** 4469
- [7] Huang X M H 2004 *PhD Thesis* Caltech
- [8] Remtema T and Lin L W 2001 *Sensors Actuators A* **91** 326
- [9] Syms R R A 1998 *J. Microelectromech. Syst.* **7** 164
- [10] Carr D W, Evoy S, Sekaric L, Craighead H G and Parpia J M 1999 *Appl. Phys. Lett.* **75** 920
- [11] Yang Y T, Ekinici K L, Huang X M H, Schiavone L M, Roukes M L, Zorman C A and Mehregany M 2001 *Appl. Phys. Lett.* **78** 162
- [12] Zorman C A *et al* 1995 *J. Appl. Phys.* **78** 5136
- [13] Cleland A N and Roukes M L 1996 *Appl. Phys. Lett.* **69** 2653
- [14] Cleland A N and Roukes M L 1999 *Sensors Actuators A* **72** 256
- [15] Cleland A N and Roukes M L 1998 *Nature* **392** 160
- [16] Huang X M H, Manolidis M, Jun S C and Hone J 2005 *Appl. Phys. Lett.* **86** 143104
- [17] Bhiladvala R B and Wang Z J 2004 *Phys. Rev. E* **69** 036307
- [18] Ekinici K L, Yang Y T, Huang X M H and Roukes M L 2002 *Appl. Phys. Lett.* **81** 2253
- [19] Bokaian A 1990 *J. Sound Vib.* **142** 481
- [20] Haberman R 1998 *Elementary Applied Partial Differential Equations* (Englewood Cliffs, NJ: Prentice-Hall)
- [21] Goldberg Y, Levinshtein M E and Romyantsev S L 2001 *Properties of Advanced Semiconductor Materials GaN, AlN, SiC, BN, SiC, SiGe* (New York: Wiley)
- [22] Wachtman J B, Tefft W E, Lam D G and Apstein C S 1961 *Phys. Rev.* **122** 1754
- [23] Lambrecht W R, Segall B, Methfessel M and Schilfgaard M 1991 *Phys. Rev. B* **44** 3685
- [24] Cheng L F, Xu Y D and Zhang Q 2003 *CARBON* **41** 707
- [25] Neubrand A, Becker H and Tschudi T 2003 *J. Mater. Sci.* **38** 4193